LCC-0113
CBP Tech Note-276
February 2003

Linear Collider Collaboration Tech Notes

The NLC Main Damping Ring Lattice

Mark Woodley[1] and Andrzej Wolski[2]

[1]Stanford Linear Accelerator Center
Stanford University
Menlo Park, CA 04025

[2]Lawrence Berkeley National Laboratory
University of California
Berkeley, CA

Abstract: Studies of the NLC Main Damping Ring lattice since April 2001 have indicated that there are a number of collective effects that potentially limit operational performance. One possible way to reduce the impact of these effects is to raise the momentum compaction of the lattice, which requires a significant redesign. In this note, we present a lattice that has a momentum compaction four times larger than the previous design. We discuss the linear and nonlinear dynamical properties of the lattice, and present some initial estimates of the sensitivity of the new design to various magnet misalignments.

CBP Tech Note-276
LCC-0113

The NLC Main Damping Ring Lattice, February 2003

Mark Woodley
Stanford Linear Accelerator Center

Andrzej Wolski
Lawrence Berkeley National Laboratory

February 18th, 2003

Abstract

Studies of the NLC Main Damping Ring lattice since April 2001 have indicated that there are a number of collective effects that potentially limit operational performance. One possible way to reduce the impact of these effects is to raise the momentum compaction of the lattice, which requires a significant re-design. In this note, we present a lattice that has a momentum compaction four times larger than the previous design. We discuss the linear and nonlinear dynamical properties of the lattice, and present some initial estimates of the sensitivity of the new design to various magnet misalignments.

1 Introduction

The lattice design for the NLC Main Damping Rings (MDRs) reported in April 2001[1] met the specified criteria for damping rate, natural emittance and dynamic aperture (using a linear model for the damping wiggler). Subsequent studies showed that the expected nonlinearities in the wiggler field should not limit the injection efficiency of the ring[2]. However, estimates indicated that a number of collective effects could limit the operational performance of the ring[3]. For example, intra-beam scattering (IBS) could lead to an increase in the transverse emittances, and the microwave instability could increase the energy spread if the vacuum chamber does not meet the demanding impedance specification. Studies of coherent synchrotron radiation suggested that the lattice parameters were close to an instability threshold. These and other effects are sensitive to the momentum compaction of the lattice, either through the phase slip limiting the build-up of coherent modes in the bunch, or through the reduced charge density that comes with a longer bunch. It was therefore proposed to re-design the lattice to increase the momentum compaction. This could be achieved without compromising the natural emittance by reducing the field in the arc dipoles while maintaining the same bending angle. The larger dispersion generates a larger momentum compaction, while the increased value of the H-function (normally leading to a larger natural emittance) is offset by the reduced quantum excitation resulting from the lower dipole field. An undesired consequence of the lower field is the lower energy loss per turn in the dipoles, and an increased wiggler length must compensate this. Since studies of the nonlinear dynamics in the wiggler have suggested that the wiggler should not limit the dynamic aperture, some increase in length is acceptable.

2 Design Considerations

A systematic approach to the design of damping rings is described elsewhere[4]. Here, we simply outline some of the goals of the new design.

- The natural emittance and damping times are designed for an injected normalized rms emittance of 150 μm, and repetition rate 120 Hz. This includes a 50% margin on the nominal injected beam emittance of 100 μm, to allow, for example, for injection jitter filamenting into the transverse phase space.
- The lattice has four arcs composed of detuned theoretical minimum emittance (TME) cells, with four insertion straights. The damping wigglers occupy two opposite straights, while the two remaining straights accommodate the injection/extraction systems, circumference correction chicane and RF cavities. The use of four straights creates a flexible geometry. For example, changes to the length of the wiggler straight can be made without affecting the injection/extraction straights.
- To raise the thresholds or reduce the impact of a range of collective effects, the momentum compaction has been increased by roughly a factor of four, compared to the April 2001 lattice. The RF voltage has also been increased so that the RF acceptance is larger and the slope at the synchronous phase is more linear. The net result is that the bunch length has increased by less than a factor of two, from 3.7 mm to close to 5.5 mm.
- The increase in momentum compaction has been achieved by reducing the dipole main field from 1.2 T to 0.67 T (the gradient in the dipole has also been reduced, from –6.6 T/m to –2.1 T/m). The length of the dipole has increased from 0.96 m to 2.0 m. To achieve the same damping, the total length of the wiggler has increased from 46.2 m to 61.6 m. The *nominal* peak field has been kept fixed at 2.15 T, but a more accurate model of the wiggler field has been used, based on the present field map. The wiggler model in the lattice includes the horizontal and vertical focusing and integrated field that are consistent with the field map.
- The vertical tune has been moved closer to the half integer, to reduce the sensitivity to magnet misalignments.

3 Lattice Parameters

The "external" parameters driving the lattice design are shown in Table 1. The principal lattice parameters, compared with the April 2001 lattice, are shown in Table 2.

Table 1: "External" parameters.

Bunches per train	N_b	192
Bunch-to-bunch spacing	τ_b /ns	1.4
Kicker rise/fall time	τ_k /ns	65
Collider repetition rate	f /Hz	120
Injected horizontal/vertical emittance	$\gamma\varepsilon_{inj}$ /mm mrad	150
Extracted horizontal emittance	$\gamma\varepsilon_{x,ext}$ /mm mrad	<3
Extracted vertical emittance	$\gamma\varepsilon_{y,ext}$ /mm mrad	<0.02

Table 2: Principal lattice parameters.

		April 2001	February 2003
Energy	E /GeV	1.98	1.98
Number of bunch trains stored	N_{train}	3	3
Vertical store time [a]	N_τ	4.97	6.11
Circumference	C /m	299.792	299.792
Arc cell type		TME	TME
Arc cell length	/m	5.120	4.908
Length of wiggler straight(s)	/m	62.856	2×49.297
Length of injection straight(s)	/m	62.856	2×22.468
Number of arc cells		34 + 4×½	28 + 8×½
Main arc dipole field	/T	1.20	0.670
Main arc dipole gradient	k_1 /m^{-2}	-1.0	-0.315
Matching arc dipole field	/T	1.20	0.373
Matching arc dipole gradient	k_1 /m^{-2}	-1.30	-0.671
Betatron tunes	Q_x, Q_y	27.2616, 11.1357	21.150, 10.347
Natural chromaticity	ξ_x, ξ_y	-37.12, -28.24	-30.74, -28.76
Normalized natural emittance	$\gamma\varepsilon_0$ /μm rad	2.17	2.37
Damping times	τ_x, τ_y, τ_ε /ms	4.85, 5.09, 2.61	3.63, 4.08, 2.18
Extracted horizontal emittance	$\gamma\varepsilon_{x,ext}$ /μm rad	2.18	2.37
Equilibrium vertical emittance	$\gamma\varepsilon_{y,equ}$ /pm rad	0.013	0.019
Extracted vertical emittance	$\gamma\varepsilon_{y,ext}$ /μm rad	0.019	0.020
Momentum compaction	α	0.295×10^{-3}	1.388×10^{-3}
RF frequency	f_{RF} /MHz	714	714
Harmonic number	h	714	714
RF voltage	V_{RF} /MV	1.07	2.0
Number of RF cavities		3	5
RF acceptance	ε_{RF}	1.5 %	1.52 %
Rms energy spread	σ_δ	0.0909 %	0.0975 %
Natural Bunch length	σ_z /mm	3.60	5.49
Synchrotron tune	Q_s	0.003496	0.0118
Wiggler peak field	$\hat{B}_w$ /T	2.15	2.15
Wiggler period	λ_w /m	0.27	0.27
Wiggler total length	L_w /m	46.238	61.568
Integrated wiggler field	$\int \hat{B}_w^2 \mathrm{d}s$ /T^{2}m	106.866	168.1 [b]
Energy loss/turn from dipoles	U_0 /keV	247	136
Energy loss/turn from wiggler	U_w /keV	530	834
Total energy loss/turn	$U_0 + U_w$ /keV	777	970
Energy loss ratio	$F_w = U_w / U_0$	2.15	6.13

[a] The vertical store time is the number of vertical damping times for which each train is stored.
[b] Determined from wiggler field map, and includes end poles and non-sinusoidal variation of the field.

The synchrotron radiation integrals, damping partition numbers and mean beta functions are given in Table 3.

Table 3

Synchrotron radiation integrals and averaged lattice parameters in the April 2001 and February 2003 lattices.

	April 2001	February 2003
I_1	0.08846 m	0.41604 m
I_2	3.6592 m^{-1}	4.4812 m^{-1}
I_3	1.0237 m^{-2}	1.3885 m^{-2}
I_4	-0.18977 m^{-1}	-0.55623 m^{-1}
I_5	3.8337×10^{-4} m^{-1}	5.3552×10^{-4} m^{-1}
J_x	1.0519	1.1241
J_y	1	1
J_ε	1.9481	1.8759
$\langle\beta_x\rangle$	3.64 m	3.97 m
$\langle\beta_y\rangle$	7.06 m	6.89 m
$\langle H_x\rangle$	0.00191 m	0.00309 m

Lattice functions for different sections of the lattice are shown in Figure 1 through Figure 6 below. Note that the main arc dipoles have a horizontally defocusing gradient, with a normalized value $k_1 = -0.32$ m^{-2} (gradient –2.1 T/m). Also, the horizontally focusing quadrupoles in the arc cells have a small horizontal offset, to provide some bending (in the opposite direction to the main dipoles). This is necessary in a highly compact TME cell to tune the dispersion and horizontal beta function for low emittance. Without this extra bending, the ability to vary the dispersion and beta function independently is very limited. The parameters for the offset magnets (those in the matching cells into the straights require a different gradient to those in the main arc cells) are given in Table 4. The required offset of the quadrupole is approximately 10% of the pole-tip radius, and the field quality in this region will need to be considered carefully.

Table 4

Parameters of offset quadrupoles in the arc cells.

Magnet name	QF	QFM
Location	Main arc	Matching into straights
Length	0.25 m	0.25 m
Gradient	27.73 Tm^{-1}	30.40 Tm^{-1}
Bending angle	2.729 mrad	2.729 mrad
Dipole component	0.07211 T	0.07211 T
Horizontal beam offset	2.60 mm	2.37 mm

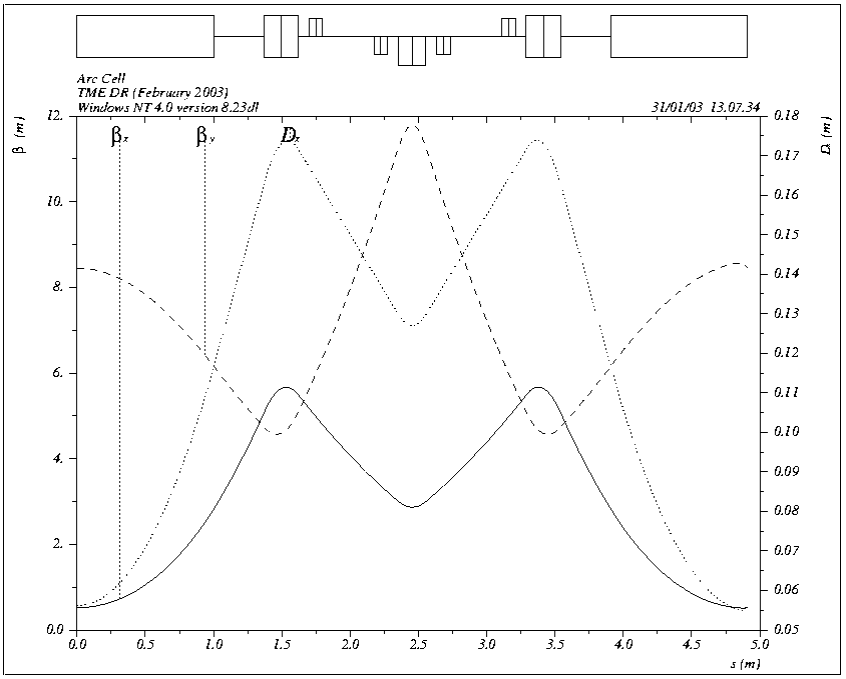

Figure 1

Lattice functions in an arc (TME) cell. Note that the horizontally focusing quads are offset to provide a small amount of bending, and are represented in the deck as combined function dipoles.

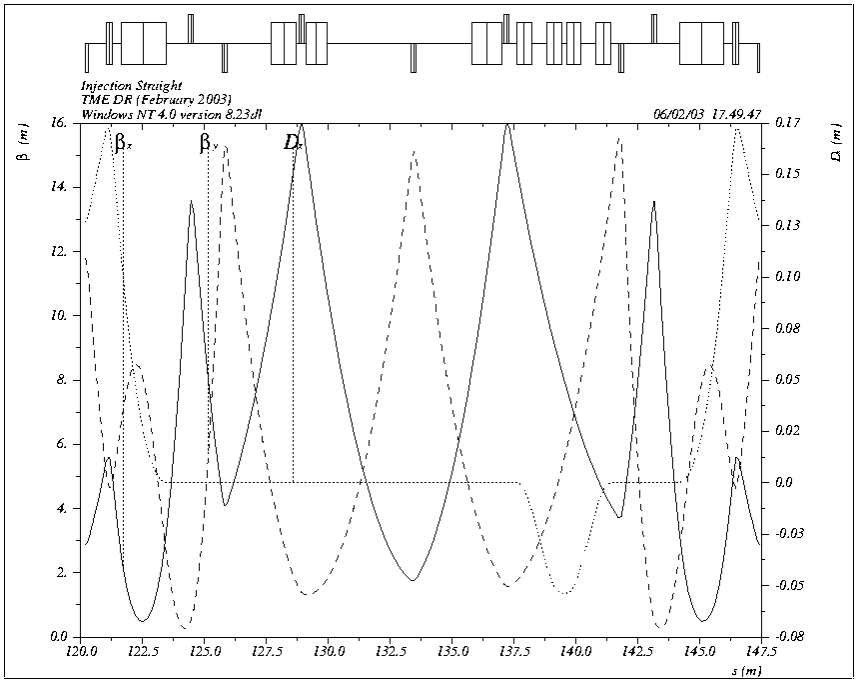

Figure 2

Lattice functions in the injection straight. The chicane is to the right (downstream) of the injection kicker, and is tuned to the nominal setting (magnets at half strength), giving some negative dispersion.

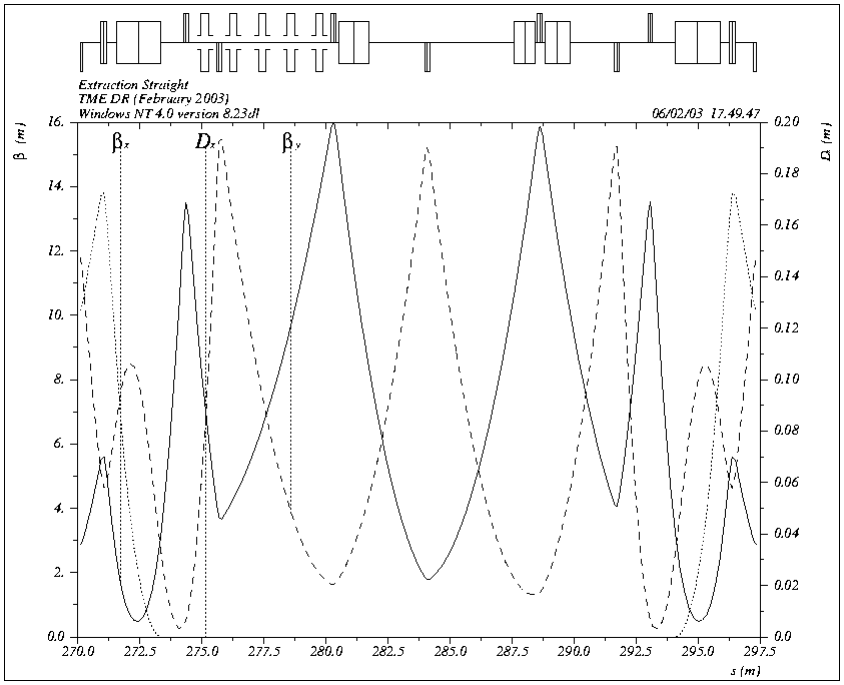

Figure 3

Lattice functions in the extraction straight. The RF cavities are to the left (upstream) of the extraction kicker.

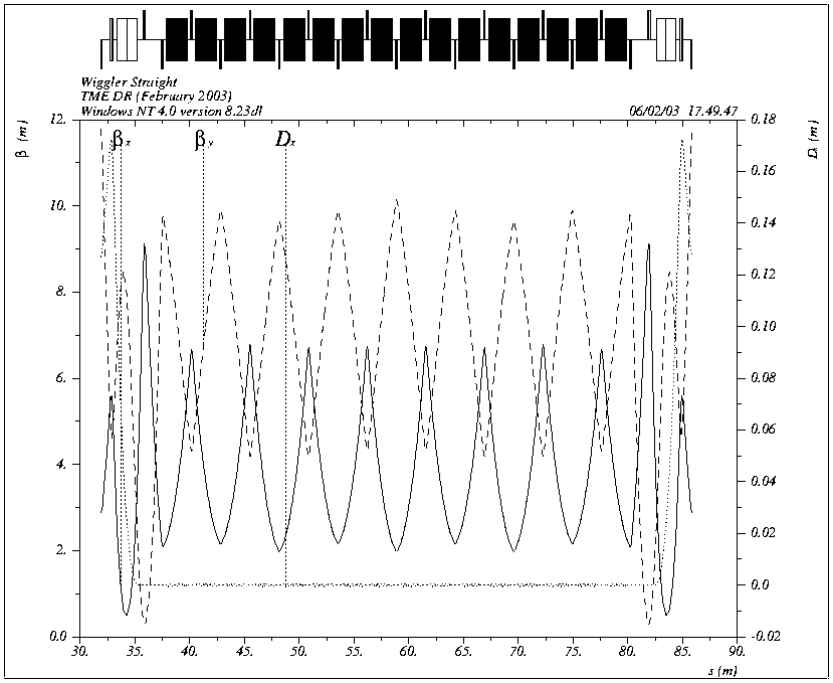

Figure 4

Lattice functions through the wiggler straight. The apparent "beta beating" results from the independent tuning of different quadrupoles, to allow control of the global tune of the lattice.

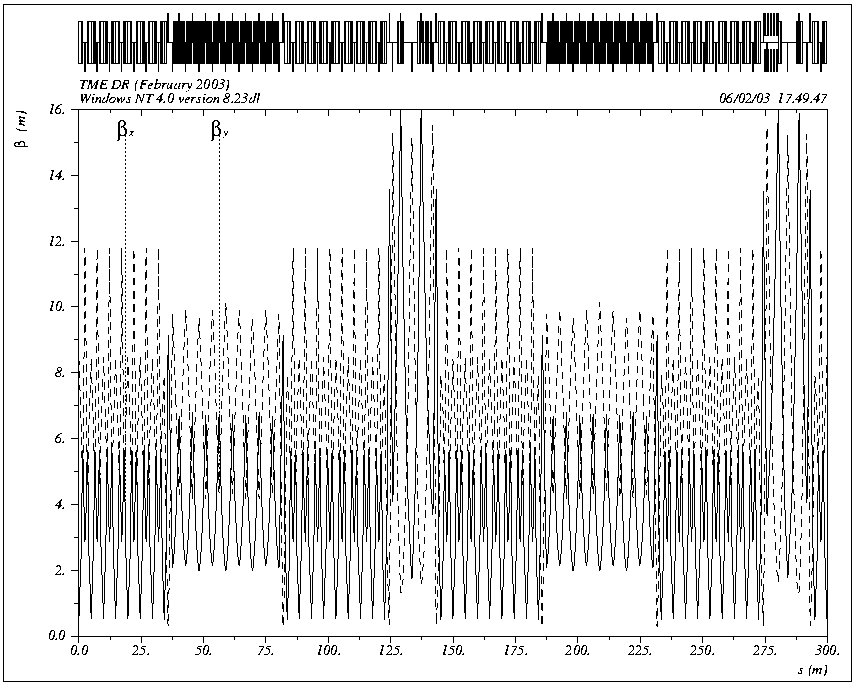

Figure 5

Beta functions for the complete lattice.

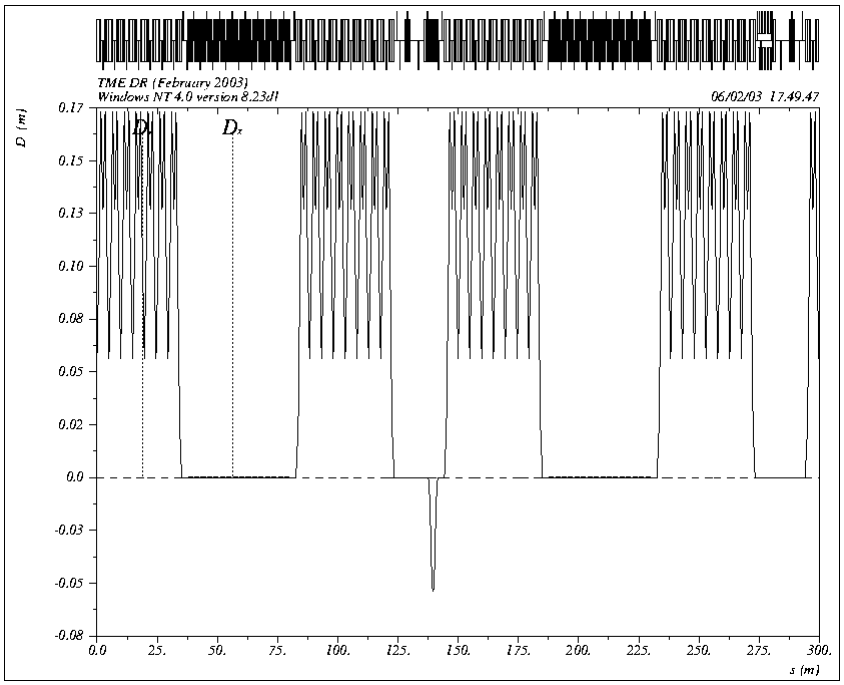

Figure 6

Dispersion function through the complete lattice.

Note that the total circumference is slightly larger than the 298.95 m minimum required to accommodate three bunch trains (192 bunches at 1.4 ns separation) with 65 ns kicker rise/fall time; the additional circumference was required to meet the constraints on beta

functions and phase advances in the straight sections. However, the difference between the actual and minimum circumference is less than 1%, and does not have a significant effect on the damping times or the extracted emittance. The actual circumference gives a harmonic number of 714, where the RF frequency is 714 MHz, so the revolution period is exactly 1 μs.

The footprint of the lattice is shown in Figure 7. A complete arc is shown in Figure 8, and a single arc cell in Figure 9.

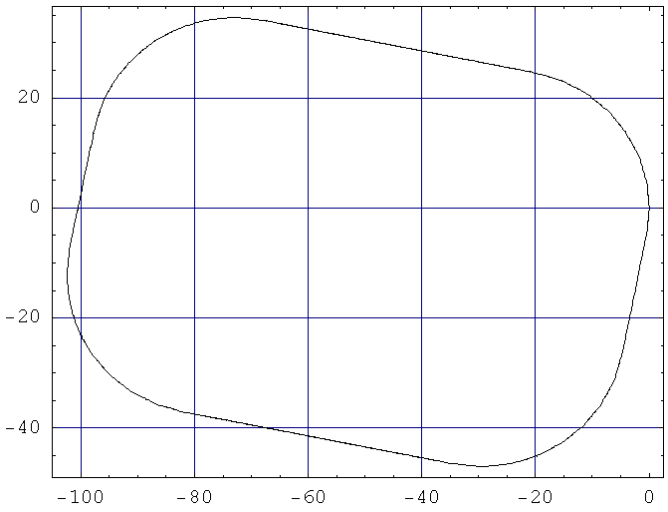

Figure 7

Footprint of the February 2003 lattice. The scales on the grid are in meters.

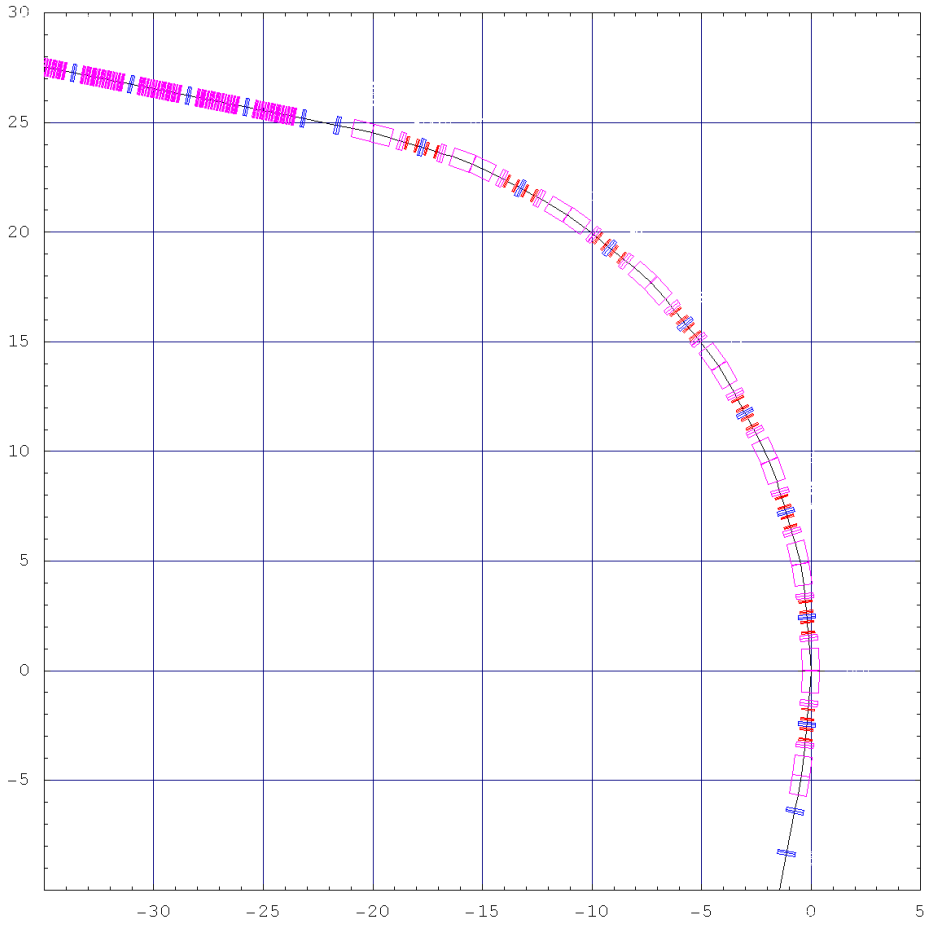

Figure 8

Layout of one arc. Bending magnets are in magenta, quadrupoles in blue and sextupoles in red.

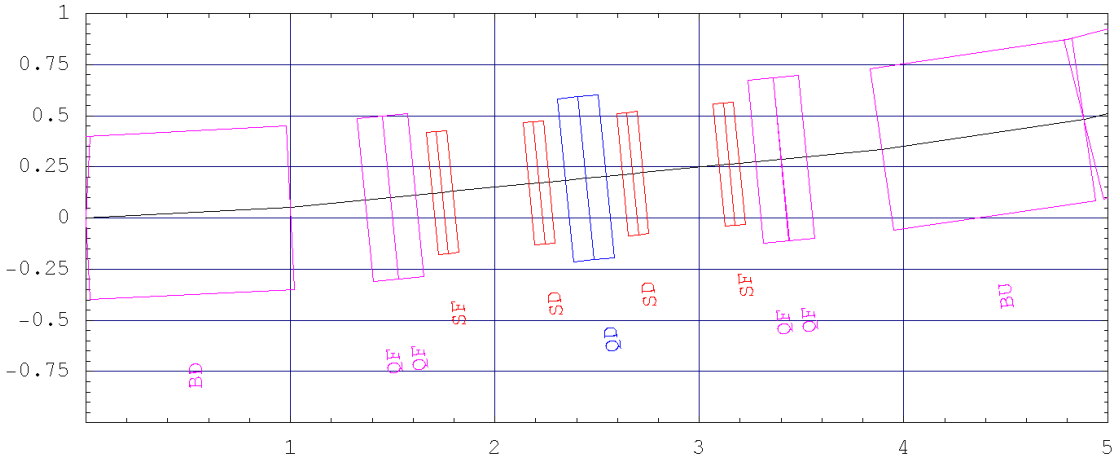

Figure 9

Layout of a single arc cell. The bending from the QF quadrupoles is less than 3 mrad, and is not visible on this scale.

4 Chromatic Properties

The sextupoles are adjusted to give zero first-order chromaticity, although there remains a residual tune shift with momentum, as a result of higher order chromaticity. The variation of horizontal and vertical tune with momentum deviations up to ±1.5% are shown in Figure 10, and the working point in tune space is shown in Figure 11.

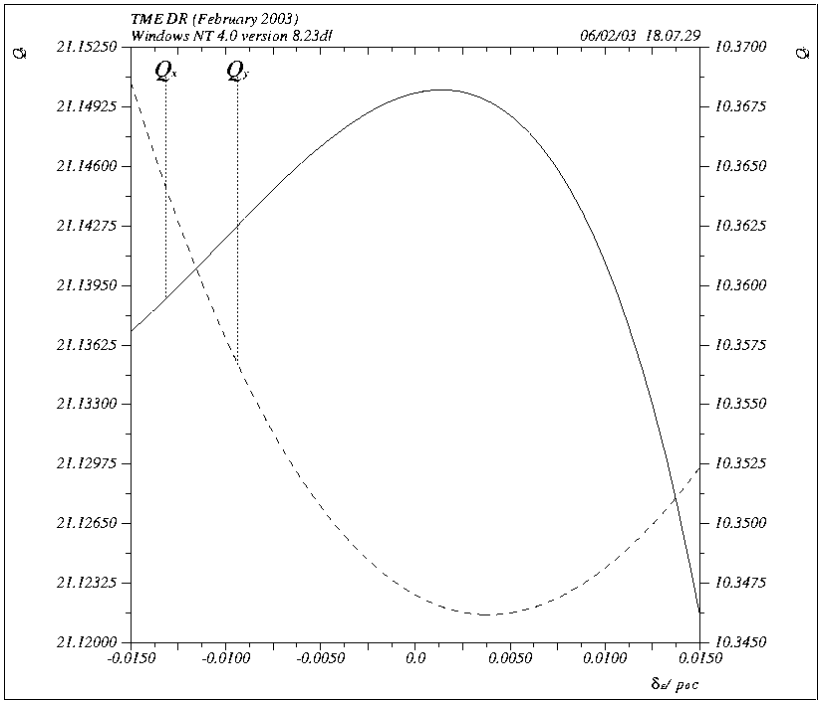

Figure 10

Variation of tunes with momentum, up to ±1.5% momentum deviation.

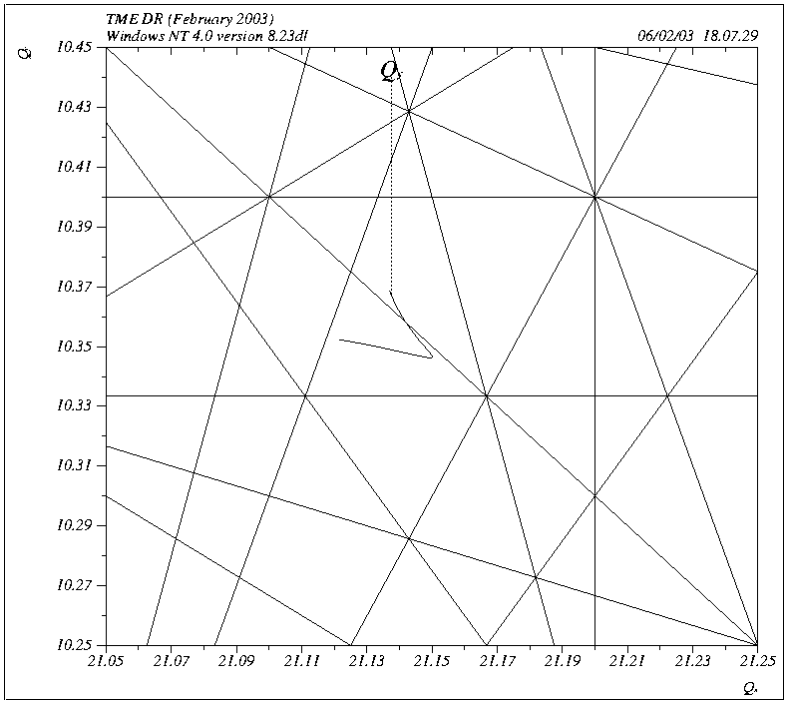

Figure 11

Working point of the lattice in tune space. The working point line shows variation of the tune with momentum deviations up to ±1.5%. Resonance lines up to fifth order are shown.

5 Dynamic Aperture

The damping ring must have a good dynamic aperture to minimize particle loss, particularly during injection. The aperture is limited by nonlinear lattice elements, in particular the sextupoles, which are used in the dispersive regions (the arcs) to correct chromaticity, and tuned to give the lattice zero chromaticity. The nominally linear elements, such as the dipoles, quadrupoles and wiggler, may also have nonlinear components as a result of systematic and random field errors; these will also affect the dynamic aperture, and the allowable reduction in the aperture is a consideration for setting the tolerances on the field quality in these elements. For the present, however, we consider only nonlinear effects arising from the sextupoles, and from an octupole component in the wiggler.

The lattice has been tuned with some efforts made to optimize the phase advances over different sections, namely the arc cells, and the wiggler and injection/extraction straights. In the arc cells, the lattice functions were controlled to give suitable locations for chromatic sextupoles, i.e. locations with large dispersion and good separation of the horizontal and vertical beta functions. The tunes of a single arc cell were chosen to give good dynamic aperture for a lattice constructed entirely from arc cells. The straights were tuned starting from integer phase advances in both planes (to maintain the symmetry of the lattice), with some detuning from this condition to reduce the chromaticity of the straights and empirically improve the dynamic aperture of the full lattice.

The two families of sextupoles are tuned to give zero first-order chromaticity. The only other explicitly non-linear term included in the lattice at present is an octupole component in the wiggler. Recent analysis of the field map for the NLC Main Damping Ring wiggler has suggested that the third-order dependence of the transverse kicks on the transverse co-ordinates may be represented by an octupole component in a single period of this device with integrated strength $k_3 l \approx 100$ m^{-3}. It is important to note that not only is there significant uncertainty in this value, but that the octupole component is only a crude representation of the nonlinear dynamics in the wiggler. For example, it is clear from Figure 17 below that the octupole term does not exactly reproduce the correct dynamics in both planes simultaneously. The problem of accurately representing the wiggler dynamics in a tracking code is the focus of work in progress[5]. We give some further discussion below of the wiggler model we have used.

Horizontal and vertical phase space portraits for the full lattice are shown in Figure 12 (no octupole component in the wiggler) and Figure 13 (including an integrated octupole component of 100 m^{-3} per wiggler period).

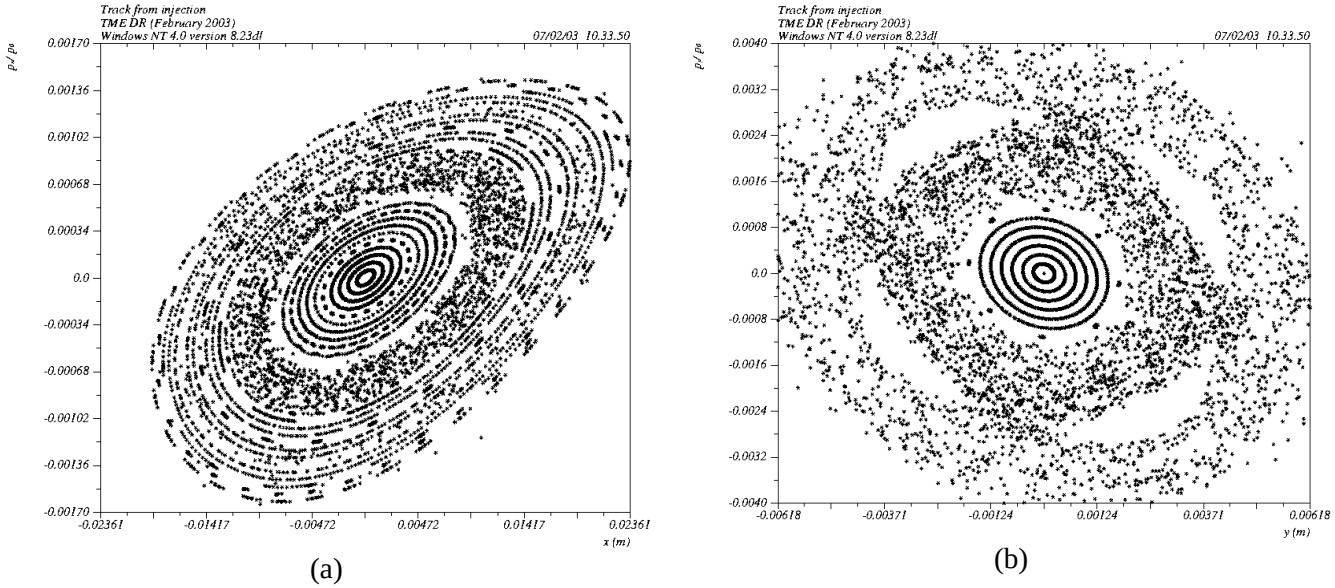

(a) (b)

Figure 12

(a) Horizontal and (b) vertical phase space portraits at the center of the first quadrupole after the injection kicker (β_x = 16.0 m, α_x = -0.573, β_y = 1.579 m, α_y = 0.154), with no octupole component in the wiggler. The particles are launched at steps of the injected beam size, assuming a normalized injected emittance of 150 μm. For the horizontal phase space, the particles are launched with a small (0.5 mm) vertical amplitude.

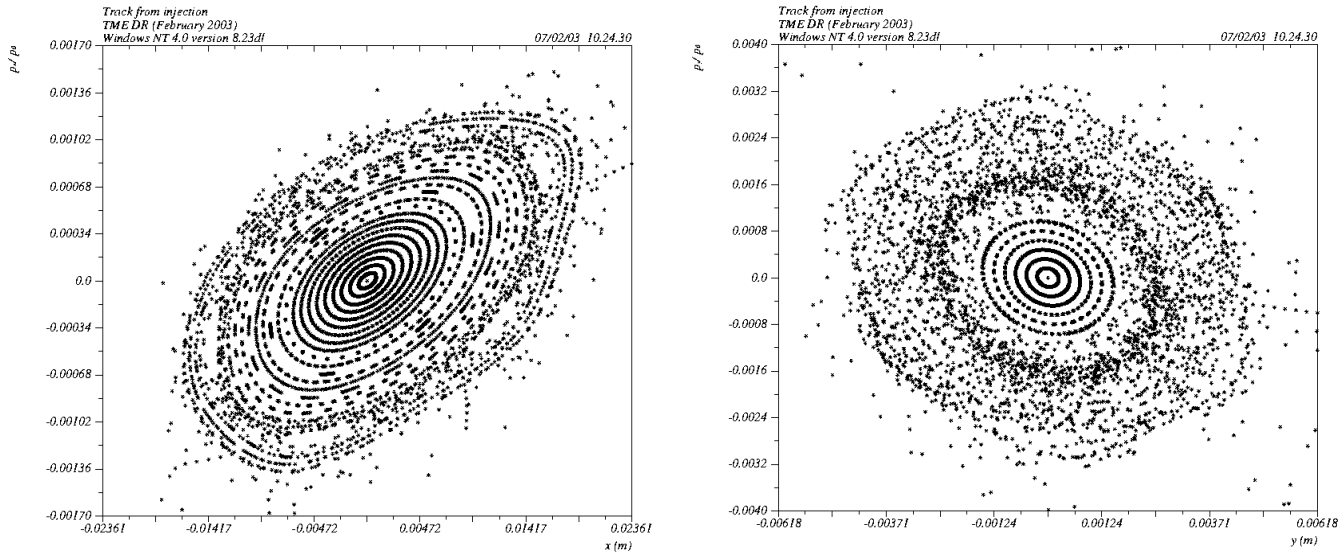

(a) **(b)**

Figure 13

(a) Horizontal and (b) vertical phase space portraits at the center of the first quadrupole after the injection kicker, with an integrated octupole component of 100 m^{-3} per wiggler period. The starting conditions and scales are the same as in Figure 12.

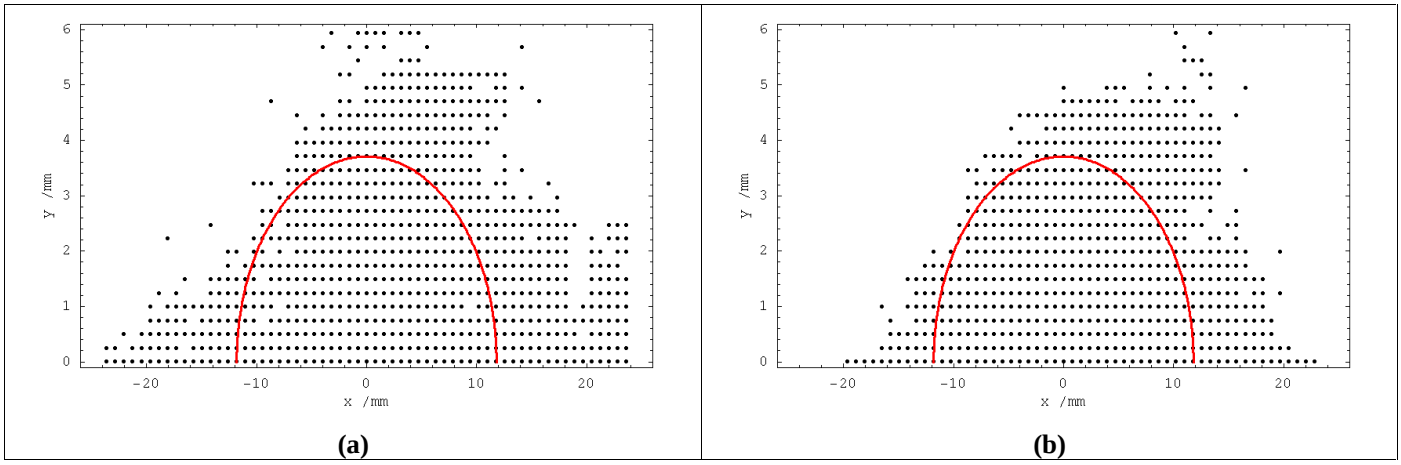

(a) **(b)**

Figure 14

Dynamic aperture for on-momentum particles using (a) a linear wiggler model and (b) an integrated octupole component of 100 m^{-3} per wiggler period. The particles were tracked through 500 turns, with the observation point at the center of the first quadrupole after the injection point. The points are separated by the injected beam size, and the half ellipse shows 15 times the injected beam size.

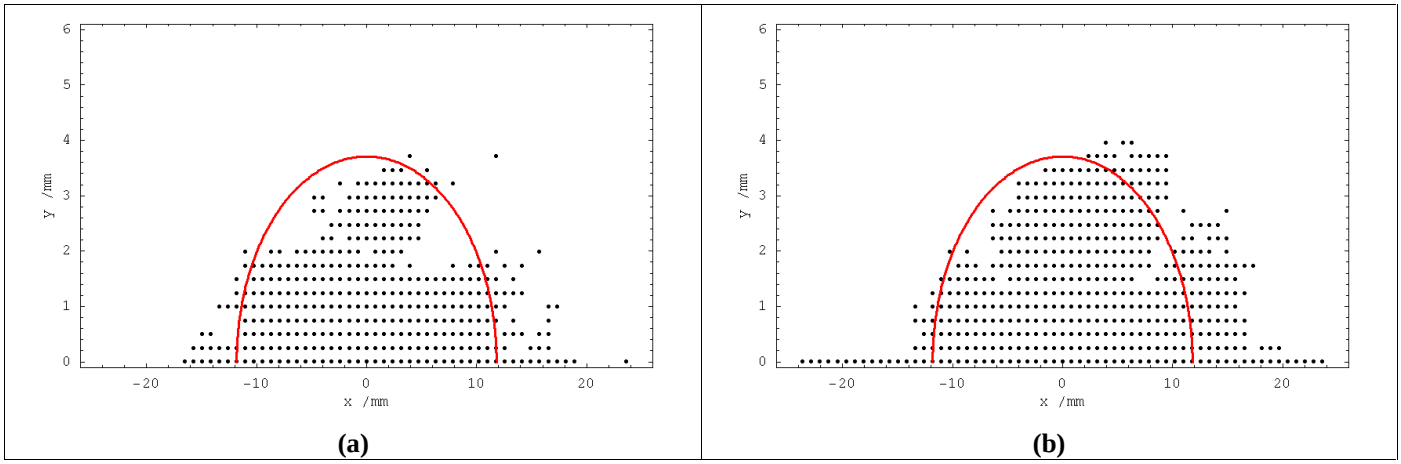

Figure 15

Dynamic aperture with a wiggler model including the octupole component, and for momentum deviations (a) -1.0% and (b) +1.0% using the same conditions as Figure 14.

On-momentum dynamic aperture plots for the full lattice (first with a linear wiggler model and then with a wiggler including an octupole component) are shown in Figure 14. We emphasize that the nonlinear model for the wiggler is only a rough approximation, and there are no systematic or random field errors or gradient errors on the dipoles, quadrupoles or sextupoles. Figure 15 shows the dynamic aperture for particles with ±1.0% momentum deviation and including the octupole component in the wiggler. Although the dynamic aperture falls within the fifteen times injected beam size specified for on-momentum particles, we feel there is still sufficient margin. More detailed studies are needed to determine the real acceptance of the storage ring, including the physical aperture and significant errors.

6 Wiggler Model

The field map we have used for the wiggler is the same as that used previously. For analysis of the dynamics in the wiggler, we have fitted the coefficients of a cylindrical mode representation of the field:

$$B_\rho = \sum c_{mn} I'_m(nk_z\rho)\sin(m\phi)\cos(nk_z z)$$

$$B_\phi = \sum c_{mn} \frac{m}{nk_z\rho} I_m(nk_z\rho)\cos(m\phi)\cos(nk_z z)$$

$$B_z = -\sum c_{mn} I_m(nk_z\rho)\sin(m\phi)\sin(nk_z z)$$

where $I_m(x)$ are modified Bessel functions of the first kind. The coefficients are found by selecting a reference radius, and performing a two-dimensional Fourier transform on the radial field component in the azimuthal and longitudinal variables. It can be shown that this procedure smooths the field and reduces the fitting errors inside the reference radius[6]. Choosing a reference radius close to the pole tip ensures a good fit for the field in the region of interest for the beam dynamics. Some sample field fits obtained for the wiggler using this technique are shown in Figure 16. The coefficients can then be used in a symplectic integrator to track through the wiggler[7,5]. Since this is a slow process for a

long wiggler, we have simply calculated the transverse kicks given to a particle entering a single period of the wiggler at different transverse co-ordinates, and developed a model using standard elements in MAD8 that (approximately) reproduces these dynamics. The results are shown in Figure 17.

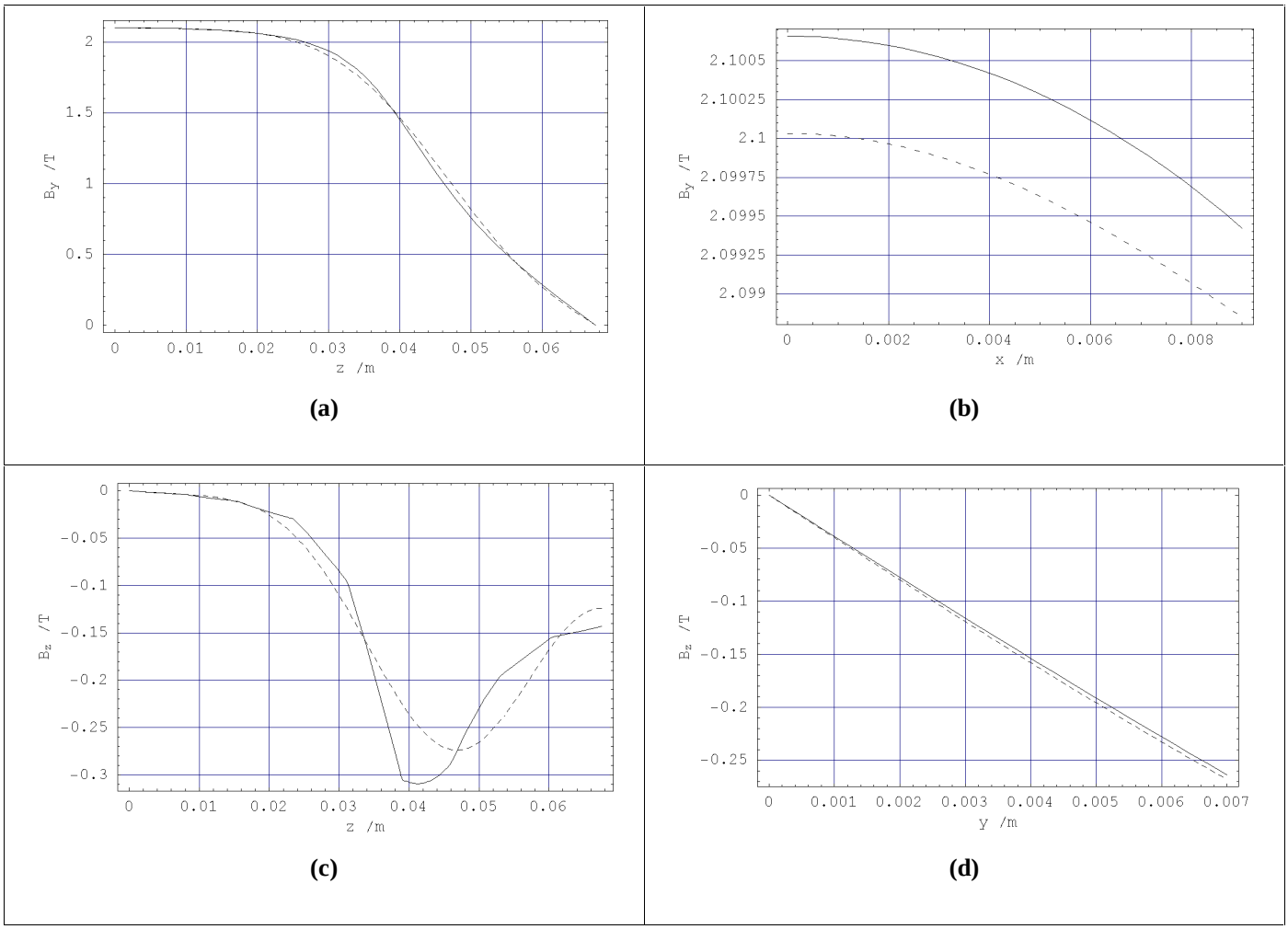

Figure 16

Sample field fits for the NLC MDR wiggler. The solid line shows the field data, and the broken line shows the fit. (a) Vertical field component vs longitudinal co-ordinate; (b) vertical field component vs horizontal co-ordinate; (c) longitudinal field component vs longitudinal co-ordinate at 4 mm vertically offset from the wiggler axis; (d) longitudinal field component vs vertical co-ordinate.

We note that as well as the third-order (octupole) component, there is some horizontal linear focusing, and the vertical focusing deviates from that expected from a sinusoidal model of the wiggler field. (The vertical focusing from a sinusoidal model is the same as that from a hard-edged dipole model of the wiggler). The horizontal linear focusing comes from the second-order roll-off of the vertical field with horizontal co-ordinate, and the third-order focusing comes from the fourth-order roll-off of the field. The variation in the vertical dynamics comes from the roll-off and from longitudinal harmonics. We find that the dynamics indicated in Figure 17 are consistent with a hard-edged dipole model, with the following modifications:

- A field gradient of –0.111 T/m is added to each pole, to give the correct horizontal focusing.
- The peak field is increased from 2.15 T by 6%. This gives an integrated squared field strength in good agreement with that calculated directly from the field map, and also, in combination with the field gradient, gives the correct linear vertical focusing.
- An thin octupole of integrated strength 100 m^{-3} is added to each wiggler period, to approximate the third-order dynamics.

The octupole component does not exactly reproduce the dynamics in both planes, and we have arbitrarily selected a value that gives a good fit for the horizontal plane. The approach we have used to modeling the wiggler is still in development[5], and will be reported in more detail elsewhere. We hope that a more rigorous study of the effect of the wiggler on the dynamic aperture of the lattice will be carried through in the near future.

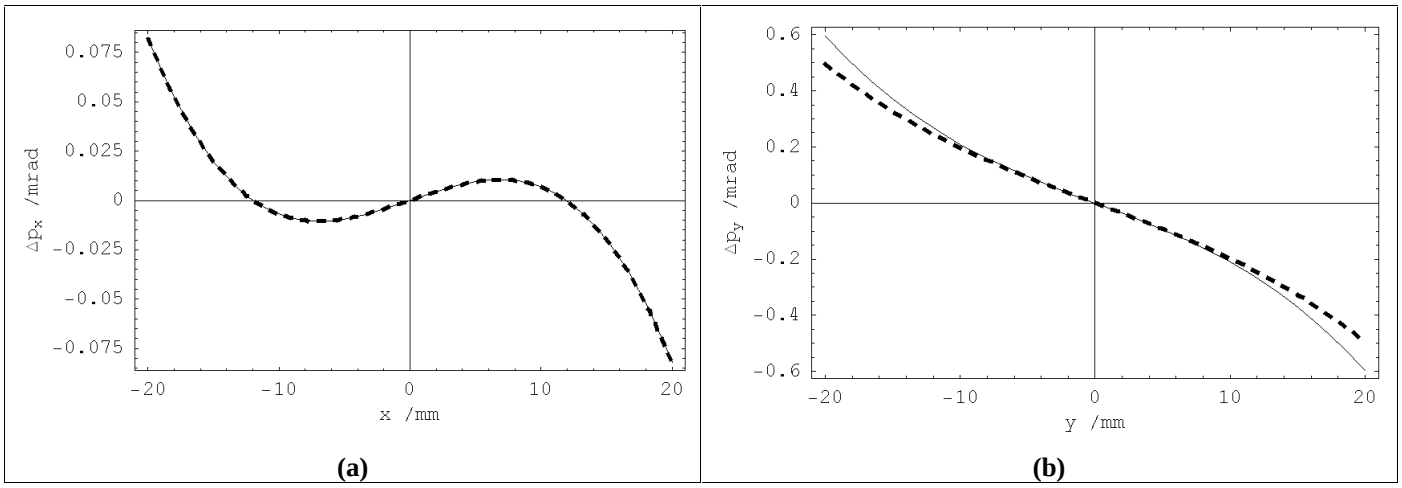

Figure 17

(a) Horizontal and (b) vertical kicks as functions of the corresponding co-ordinate in one period of the NLC MDR wiggler. The solid line shows the results from a detailed symplectic integrator, while the heavy broken line shows the results of a dipole model with quadrupole and octupole components. Note that we have extrapolated the field beyond the reference radius of 9 mm.

7 Other Systems

7.1 Circumference Correction Chicane

A chicane provides the possibility of making small corrections to the circumference without the need to adjust the RF frequency. The specified correction range, based on observations of existing rings[8], is ±2 mm, and the chicane included in the present lattice design meets this specification. The length of the chicane is 3.80 m, which allows it to fit in a 4.42 m drift section of the injection/extraction straight, with a drift of 0.31 m between the faces of the outside dipoles and the nearest quadrupoles. Each of the four chicane magnets has an effective length of 0.6 m at the nominal (half maximum) field strength of 0.492 T.

7.2 RF Cavities

An RF voltage of 2.0 MV is required to achieve a momentum acceptance of ±1.5%. Each cavity is capable of providing up to 0.5 MV, so in principle four cavities could be sufficient. However, this allows no overhead, and it might be necessary, for example, to compensate intensity-dependent bunch lengthening effects by increasing the RF voltage. We have therefore designed the lattice to accommodate five cavities. Each cavity requires approximately 1 metre of free space[9]. To avoid transients arising from variations in beam loading during injection/extraction, the cavities must be placed downstream of the injection kicker and upstream of the extraction kicker (in the present design they are positioned just before the extraction kicker). In this case, no transients are induced as long as injection occurs simultaneously with extraction.

At present, the cavities are separated by 2.25 RF wavelengths, that allows pairs of cavities to be powered by a single klystron, with the power divided in a "magic T". Thus, there are several possible configurations, using between three and five klystrons; since it is also possible to power three cavities from a single klystron, it may be possible to use just two klystrons. The optimal configuration will need further study, and we simply note at present that using one klystron for each cavity provides the greatest flexibility, and will provide some overhead, allowing the ring to continue operation (albeit with impaired performance) in the case of any one klystron failing.

7.3 Injection/Extraction

The injection/extraction components have been positioned according to space constraints and the required phase advances. The components are represented in the deck by zero-bend dipoles, of lengths as specified in the ZDR[10]. Each system consists of a kicker (1.2 m length with a kick angle of 2.5 mrad) and a pair of septa (0.83 m, 25 mrad thin blade and 1.0 m, 90 mrad thick blade). The phase advance between the kicker and the septa is close to $0.25\times 2\pi$ horizontally, so that the horizontal momentum change from the kicker is converted into a large transverse displacement at the first septum.

The extraction geometry is shown in Figure 18. Assuming a half-aperture in the zero-field region of the first septum of 20 mm (the same as in the arcs) and a blade thickness of 5 mm, there is a clearance of 2.5 mm between the trajectory of the injected/extracted beam and the septum blade. This is a rather smaller clearance than we should prefer. The injected/extracted beam passes through two quadrupoles. At Q4E it passes between 7 mm and 8 mm off-axis, receiving a kick of 3.2 mrad in the same direction as that from the kicker. At Q5E, located between the septa in the scheme shown, it passes between 45 and 50 mm off-axis, receiving a kick of 17.6 mrad in the opposite direction to that from the kicker. This magnet will need a pole-tip radius of around 60 mm, which at its nominal strength would give a pole-tip field of 0.72 T. Overall, the engineering design of the injection/extraction regions (bearing in mind the need for a low impedance vacuum chamber) is likely to present some challenges, though it might be possible to modify the septum lengths and fields to make things easier. For example, an alternative geometry is shown in Figure 19. The only change from Figure 18, is that the length and kick angle of the first septum have been reduced by half. The clearance at the blades of both septa is now 4 mm, and the pole tip radius of Q5E is 52 mm, and the pole tip field has been reduced to 0.624 T. The total kick angle of the system is 94 mrad as opposed to 103 mrad in the previous case.

The apertures through the zero-field regions of the septa are assumed to be the same as the aperture in the arcs to avoid the need for transitions that may add to the impedance. Engineering studies are needed to determine the best configuration.

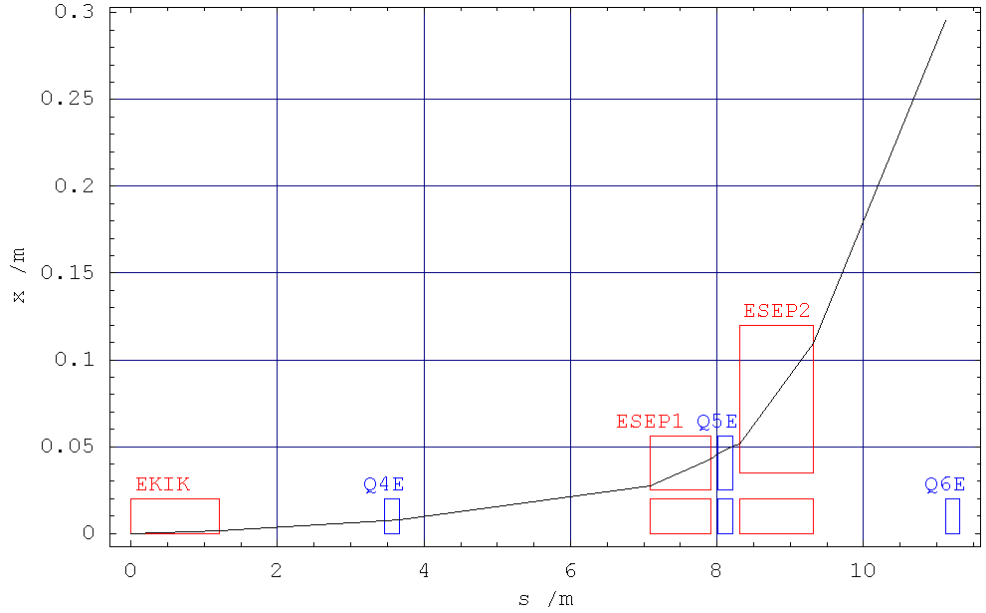

Figure 18

Geometry of the extraction system. The rectangles represent the nominal length and aperture of the quadrupoles, extraction kicker and septa. The first septum applies a 25 mrad kick and has a 5 mm blade thickness. The second septum applies a 90 mrad kick, and has a 15 mm blade thickness.

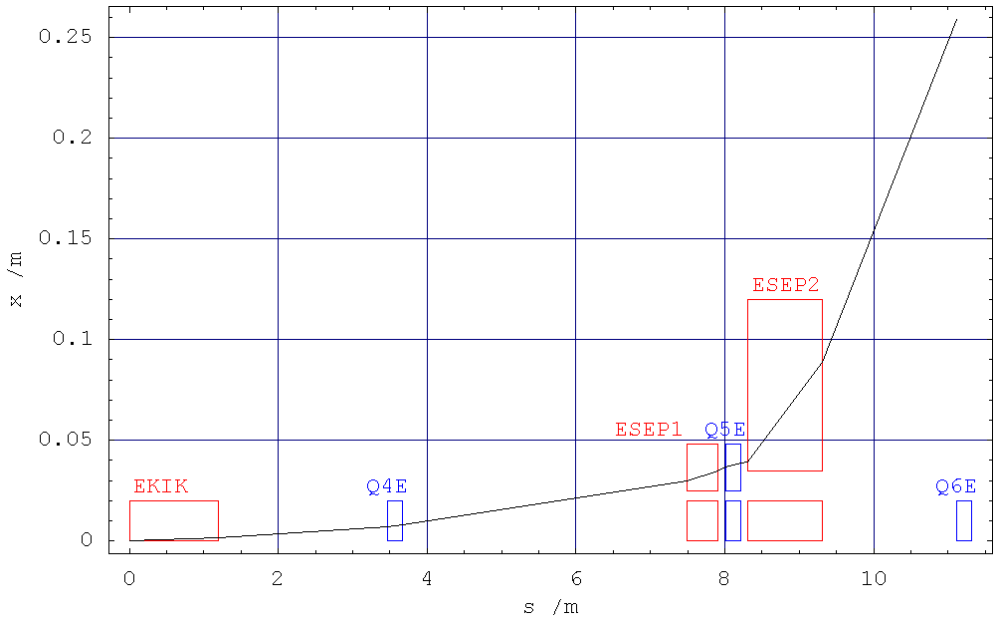

Figure 19

As Figure 18, but with the length and kick angle of the first septum reduced by half.

Other options for the layout of the injection/extraction scheme may be based on the use of a septum quadrupole for Q5E, where the injected/extracted beam sees a zero-field region of the magnet. Such a magnet has been used for example in the interaction region of PEP-II[11].

The rise/fall time of the kickers is assumed to be 65 ns, which is slightly less than the gap between bunch trains, though it is to be expected that the following stored train will see some of the falling edge of each kicker. In the previous lattice design, a half-integer phase advance separated the kickers, so that the pulse of the second kicker could be shaped to compensate for errors arising from the trailing edge of the first. Unfortunately, space constraints in the present lattice design preclude this arrangement.

7.4 Vacuum Chamber Aperture

The dipoles, quadrupoles and sextupoles have achievable pole-tip fields if the pole-tip radius is assumed to be 25 mm. This allows a possible increase in the internal diameter of the vacuum chamber outside the wiggler straights from 32 mm (April 2001 lattice) to 40 mm, with 3 mm wall thickness and 2 mm clearance. Increasing the vacuum chamber aperture has the benefit of assisting the achievement of low vacuum pressure, and also reduces the strength of the resistive wall wake fields, which are expected to drive coupled bunch instabilities[3].

Unfortunately, the wiggler sections still require a narrow 16 mm internal diameter vacuum chamber.

8 Initial Estimates of Alignment Sensitivities

The attainment of very low vertical emittance will be a key performance measure of the Main Damping Rings. Vertical emittance comes from vertical dispersion and betatron coupling. To get an idea of the response to misalignments of the present lattice compared to the previous design, we can make some simple estimates of the sensitivity of the emittance to *uncorrelated* sextupole misalignments and quadrupole rotations, both of which types of misalignments generate vertical dispersion and betatron coupling.

The vertical emittance from uncorrelated sextupole misalignments may be written:

$$\varepsilon_y \approx \left\langle \Delta Y^2_{\text{sextuple}} \right\rangle \cdot \left[\Sigma_{2C} \frac{J_x \left(1 - \cos 2\pi\nu_x \cos 2\pi\nu_y\right)}{4J_y \left(\cos 2\pi\nu_x - \cos 2\pi\nu_y\right)^2} \varepsilon_x + \Sigma_{2D} \frac{J_\varepsilon \sigma_\delta^2}{4\sin^2 \pi\nu_y} \right]$$

and the vertical emittance from uncorrelated quadrupole rotations may be written:

$$\varepsilon_y \approx \left\langle \Delta\Theta^2_{\text{quadrupole}} \right\rangle \cdot \left[\Sigma_{1C} \frac{J_x \left(1 - \cos 2\pi\nu_x \cos 2\pi\nu_y\right)}{J_y \left(\cos 2\pi\nu_x - \cos 2\pi\nu_y\right)^2} \varepsilon_x + \Sigma_{1D} \frac{J_\varepsilon \sigma_\delta^2}{\sin^2 \pi\nu_y} \right]$$

where the “magnet sums” are given by:

$$\Sigma_{2C} = \sum_{\text{sextupoles}} \beta_x \beta_y (k_2 l)^2$$

$$\Sigma_{2D} = \sum_{\text{sextupoles}} \beta_y (k_2 l \eta_x)^2$$

$$\Sigma_{1C} = \sum_{\text{quadrupoles}} \beta_x \beta_y (k_1 l)^2$$

$$\Sigma_{1D} = \sum_{\text{quadrupoles}} \beta_y (k_1 l \eta_x)^2$$

The values of the summations for the previous and present lattices are given in Table 5.

Table 5

"Magnet sums" for present and previous NLC MDR lattices.

	April 2001	February 2003
Σ_{2C}	5.54×10^5 m^{-2}	5.25×10^5 m^{-2}
Σ_{2D}	1300 m^{-1}	2890 m^{-1}
Σ_{1C}	1930	1670
Σ_{1D}	2.94 m	7.81 m
Σ_{1O}	740 m^{-1}	443 m^{-1}

We can define the sensitivity as the rms misalignment that *on its own* will generate the specified equilibrium vertical emittance. The values for the April 2001 and February 2003 lattices are given in Table 6. Note that because of the gradient in the dipoles, we have included these magnets in the quadrupole calculations. The sensitivity values may be compared to those given by Raubenheimer[12] for some other electron storage rings. The values of the magnet sums are very similar for the April 2001 and February 2003 lattices. The reasons for the looser sensitivities are a more optimum vertical tune, and the larger vertical emittance that is allowed by the faster vertical damping.

The beam stability in the presence of magnet vibration is also an important performance measure, because the extracted beam should have transverse jitter less than the beam size. We can again write down a simple expression to estimate the orbit motion in response to an uncorrelated quadrupole misalignment:

$$\left\langle \frac{y_{\text{co}}^2}{\beta_y} \right\rangle \approx \left\langle \Delta Y_{\text{quadrupole}}^2 \right\rangle \frac{\Sigma_{1O}}{8 \sin^2 \pi \nu_y}$$

where

$$\Sigma_{1O} = \sum_{\text{quadrupoles}} \beta_y (k_1 l)^2$$

We can again define a sensitivity, as the rms quadrupole vertical misalignment that *on its own* will generate an orbit jitter equal to the *equilibrium* beam size. The values for the present and previous lattices are given in Table 6. We again include the gradient dipoles in the quadrupole calculations. This time, the relaxed sensitivity is a combination of a smaller magnet sum, more optimal vertical tune, and larger equilibrium vertical beam size.

Table 6

Sensitivity estimates for vertical emittance and orbit jitter.

	April 2001	February 2003
Sextupole vertical alignment	32 μm	53 μm
Quadrupole rotation	336 μrad	511 μrad
Quadrupole vertical alignment	79 nm	264 nm

We see that the new lattice is significantly less sensitive to the misalignments considered, and the sensitivity values are in fact now very comparable to those for some existing electron storage rings with demonstrated performance[12].

9 Design Margins

The challenges in construction and operation of the damping ring make it prudent to include some margin between the specified performance and the ideal performance of a machine constructed and operating precisely as designed. In some cases, the performance specifications already include some margin. For example, the injected beam is assumed to have a normalized emittance of 150 μm, which allows a 50% margin for beam jitter on top of the nominal 100 μm emittance of the beam coming from the source. Some margins (e.g. in damping time) are easy to quantify, while others (e.g. in dynamic aperture) are not. In Table 7 we attempt to identify those parameters that include some margin, indicate the reason for or benefit of the margin, and quantify the margin where possible.

Table 7

Summary of margins between nominal and design parameter values.

Quantity	Nominal or Required Value	Design Value	Margin allowed for…
Injected emittance	100 μm	150 μm	Injection jitter, filamentation
Horizontal damping time	5 ms	3.63 ms	Variation in wiggler field
Natural emittance	3.0 μm	2.36 μm	Tuning errors, collective effects
Vertical damping time	5 ms	4.08 ms	Relaxation of coupling requirement
Equilibrium normalized vertical emittance	0.013 μm	<0.019 μm	Relaxation of alignment tolerances
Energy spread	< 0.1 %	0.0975 %	Almost no margin for collective effects
Bunch length	< 5 mm	5.5 mm	Specified value relaxed to reduce impact of collective effects
Maximum RF Voltage	2.0 MV	2.5 MV	Increased RF acceptance, control of bunch length
Circumference	298.95 m	299.79 m	Additional 1 ns (!) kicker rise/fall time
Dynamic aperture	few × injected beam size	15×injected beam size	Magnet errors, tuning errors, linearity of phase space
Energy acceptance	2% full width	2% full width	No margin
Magnet (not wiggler) pole-tip radius	20 mm	24 mm	Increase in vacuum pipe aperture

10 Summary of Magnet Parameters

A summary of the parameters for the magnets used in the present lattice design is shown in Table 8.

Table 8

Magnet parameters in present main damping ring lattice design.

Type	Name	Location	Length /m	Pole-tip Radius /m	Bend Angle /rad	Normalized Gradient	Pole-tip Field /T	Count
Dipole	B	Arc	2.0	0.025	0.20180814	-0.3153 m^{-2}	0.6575	28
Dipole	BM	Matching into straights	1.8	0.025	0.10090407	-0.6712 m^{-2}	0.3653	8
Dipole	BBC	Chicane	0.6	0.025	±0.089424	-	±0.9844	4
Quadrupole	QF	Arc	0.25	0.025	-2.7293×10^{-3}	4.198 m^{-2}	0.6932	56
Quadrupole	QFM	Matching into straights	0.25	0.025	-2.7293×10^{-3}	4.602 m^{-2}	0.7599	8
Quadrupole	QD	Arc	0.25	0.025		-4.453 m^{-2}	-0.7353	32
Quadrupole	Q1I	Injection straight	0.20	0.025		4.555 m^{-2}	0.7521	1
Quadrupole	Q2I	Injection straight	0.20	0.025		-4.542 m^{-2}	-0.7500	1
Quadrupole	Q3I	Injection straight	0.20	0.025		1.822 m^{-2}	0.3009	1
Quadrupole	Q4I	Injection straight	0.20	0.025		-2.152 m^{-2}	-0.3554	1
Quadrupole	Q5I	Injection straight	0.20	0.060		1.726 m^{-2}	0.6840	1
Quadrupole	Q6I	Injection straight	0.20	0.025		-4.192 m^{-2}	-0.6922	1
Quadrupole	Q7I	Injection straight	0.20	0.025		4.642 m^{-2}	0.7665	1
Quadrupole	Q1E	Extraction straight	0.20	0.025		4.648 m^{-2}	0.7675	1
Quadrupole	Q2E	Extraction straight	0.20	0.025		-4.203 m^{-2}	-0.6940	1
Quadrupole	Q3E	Extraction straight	0.20	0.025		1.722 m^{-2}	0.2843	1
Quadrupole	Q4E	Extraction straight	0.20	0.025		-2.139 m^{-2}	-0.3532	1
Quadrupole	Q5E	Extraction straight	0.20	0.060		1.821 m^{-2}	0.7217	1
Quadrupole	Q6E	Extraction straight	0.20	0.025		-4.544 m^{-2}	-0.7503	1
Quadrupole	Q7E	Extraction straight	0.20	0.025		4.560 m^{-2}	0.7530	1
Quadrupole	QFW	Wiggler straight	0.15	0.025		3.214 m^{-2}	0.5307	10
Quadrupole	QDW	Wiggler straight	0.15	0.025		-1.211 m^{-2}	-0.2000	10
Quadrupole	Q1WM	Wiggler straight	0.25	0.025		4.081 m^{-2}	0.6739	4
Quadrupole	Q2WM	Wiggler straight	0.15	0.025		-4.658 m^{-2}	-0.7692	4
Quadrupole	Q3WM	Wiggler straight	0.15	0.025		3.171 m^{-2}	0.5236	4
Quadrupole	Q4WM	Wiggler straight	0.15	0.025		-1.217 m^{-2}	-0.2010	4
Sextupole	SF	Arc	0.10	0.025		164.7 m^{-3}	0.3400	64
Sextupole	SD	Arc	0.10	0.025		-157.4 m^{-3}	-0.3249	64
Kicker	KIK	Injection/Extraction	1.2		0.0025			2
Septum	SEP1	Injection/Extraction	0.83		0.025			2
Septum	SEP2	Injection/Extraction	1.00		0.090			2

11 Summary of Results and Further Work

The lattice we have described in this note meets the main design criteria.

- The lattice has sufficiently fast damping and low natural emittance to meet requirements on extracted emittance.
- The dynamic aperture is in excess of fifteen times the injected beam size (for zero-momentum deviation), which should allow good injection efficiency.
- The circumference correction chicane is capable of correcting over a range ±2 mm.
- The lattice has sufficient room for RF cavities.

Items that need to be addressed include the following.

- A more rigorous and detailed analysis of the beam dynamics in the wiggler needs to be carried out.
- The effects of systematic and random field errors in the dipoles, quadrupoles, and sextupoles need to be studied.
- The possibility of further optimization of the nonlinear dynamics, leading to improvements in the dynamic aperture, should be investigated.
- Tuning simulations (including focusing errors and a range of alignment errors) need to be performed, and specifications for the correction system determined.
- Designs of the components in the injection/extraction system (including kickers, septa and possibly septum quadrupoles) need to be considered.
- Estimates must be made of the impact of a range of collective effects on the damping ring performance.

Acknowledgements

Thanks to Marco Venturini, Tor Raubenheimer and John Corlett for helpful discussions and comments.

References

[1] A. Wolski, *"Lattice Description for NLC MDRs at 120Hz"*, LCC-0061, April 2001.
[2] A. Wolski, *"Symplectic Integrators for Nonlinear Wiggler Fields"*, LCC-0062, April 2001.
[3] A. Wolski, S. de Santis *"Estimates of Collective Effects in the NLC Main Damping Rings"*, LCC-0080, May 2002. J.H. Wu reported at a meeting in July 2002 on studies of coherent synchrotron radiation in the NLC Main Damping Rings.
[4] P. Emma and T. Raubenheimer, *"A Systematic Approach to Damping Ring Design"*, Phys.Rev. ST Accel.Beams 4:021001, 2001.
[5] M. Venturini, *"Analysis of Single-Particle Dynamics in the NLC and TESLA Damping Ring Wigglers"*, in preparation.
[6] Thanks to Alex Dragt for proposing this technique to us.
[7] Various approaches are possible. See, for example: Y. Wu et al, *"Symplectic Models for General Insertion Devices"*, proceedings PAC 2001; Y. Wu et al, *"Explicit Higher Order Symplectic Integrator for s-Dependent Magnetic Field"*, to be published.
[8] P. Emma and T. Raubenheimer, *"Circumference Correction Chicanes for Damping Rings"*, proceedings PAC 1999.
[9] R.Rimmer et al, "*RF Cavity R&D at LBNL for the NLC Damping Rings*", LCC-0033, December 1999.
[10] The NLC Design Group, "*Zeroth-Order Design Report for the Next Linear Collider*", LBNL-PUB-5424, SLAC Report 474, UCRL-ID-124161, May 1996. pp.242-245.
[11] *"Conceptual Design Report for PEP-II, An Asymmetric B Factory"*, SLAC-418, June 1993, pp. 292-297.
[12] T. Raubenheimer and A. Wolski, *"Comparison of Alignment Tolernaces in the Linear Collider Damping Rings with those in Operating Rings"*, proceedings Nanobeams 2002.